# Engineering Design of Integrated III-V/SiN Quantum-well and Quantum-dot Lasers

**Emad Alkhazraji,[1] Weng W. Chow[2], Frederic Grillot,[3] John E. Bowers,[4,5] Scott E. Madaras,[2] Michael Gehl,[2] Erik Skogen,[2] and Yating Wan,[1]***

[1]*Integrated Photonics Laboratory, King Abdullah University of Science and Technology, Thuwal, Makkah Province, Saudi Arabia*
[2]*Sandia National Laboratories, Albuquerque, NM 87185-1086, USA*
[3]*LTCI, Telecom Paris, Institute Polytechnique de Paris, 91120 Palaiseau, France*
[4]*Institute for Energy Efficiency, University of California Santa Barbara, Santa Barbara, California, 93106, USA.*
[5]*Materials Department, University of California Santa Barbara, Santa Barbara, California 93106, USA.*
**yating.wan@kaust.edu.sa*

**Abstract:** Spectrally-pure lasers are paramount in various fields. Progression to Hz-level lasing linewidth in III-V/SiN lasers with quantum-dot active regions is predicted here. Using parametric studies, one can produce timely results in engineering designs. © 2023 The Author(s)

## 1. Introduction

Heterogeneous-integrated III-V/SiN lasers have achieved linewidths at the tens of kHz level and, in some cases, down to a few Hz or less [1, 2]. This significant laser linewidth reduction is attributed to the self-injection locking of the InP/Si laser to the $Si_3N_4$ microresonator [2, 3]. In such complex structures, there is a large parameter space to explore for design engineering. This paper describes a parametric study of the design of an integrated III-V/SiN distributed feedback (DFB) quantum well (QW) laser involving detailed and comprehensive modeling and multi-objective performance optimization. Owing to a more rigorous treatment of outcoupling and coupled cavities, we uncover a physical mechanism that is unique to heterogeneously integrated devices. The theory served well as an analytical tool for parametric studies to produce timely results for engineering design. Compared to QWs, quantum-dot (QD) gain medium embraces multiple favorable material properties, such as low transparency current, high-temperature robustness, and reduced sensitivity to external feedback and material defects [4]. By leveraging the theory model derived from QWs, progression to Hz-level lasing in III-V/SiN lasers with QD active regions is simulated.

## 2. Device modeling, analysis, and optimization

Fig. 1(a) shows a sketch of the coupled III-V/SiN DFB QW/QD laser under investigation. The parametric study here is enabled by following the microscopic laser theoretical formulation provided in [5] that includes a) multimode laser interaction to treat mode competition and wave mixing, b) quantum-optical contributions from spontaneous emission, and c) composite laser/free-space eigenmodes to describe outcoupling and coupling among components within an extended cavity. Both laser devices had a QW height of 8 nm, a waveguide height of 0.2 μm, a stripe width of 4.9 μm, a spontaneous emission factor of 0.003, dephasing and population relaxation rates of $10^{12}$ $s^{-1}$, a defect loss

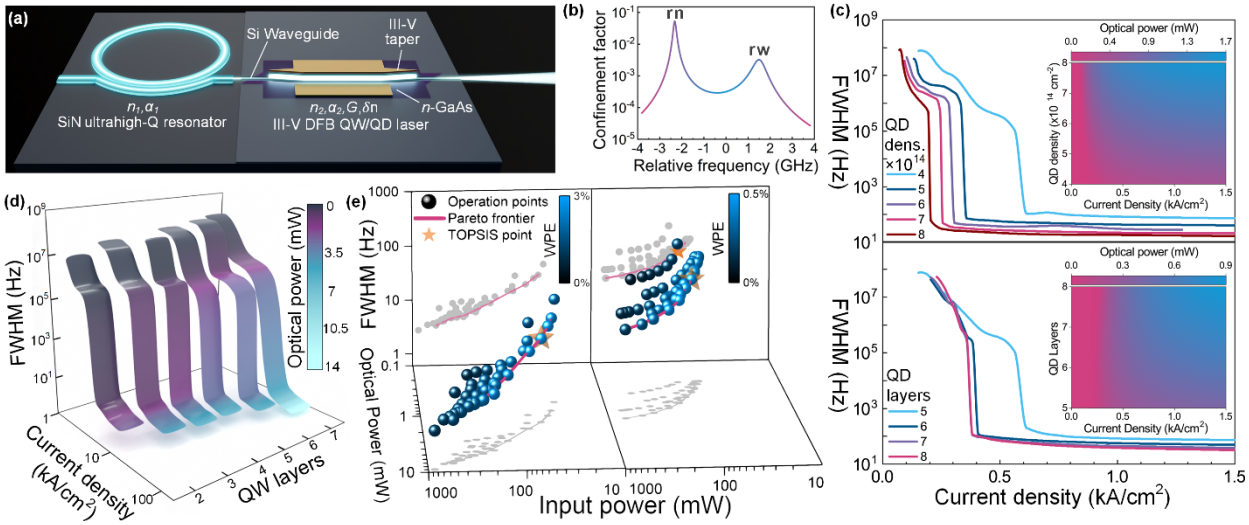


Fig. 1. (a) Sketch of the integrated III-V/SiN DFB QW/QD laser. (b) Resonces of coupled III-V and SiN cavities showing anticrossing due to optical coupling. (c) The lasing linewidth FWHM of the III-V/SiN QD laser as a function of the current density for different QD densities (top) and QD layers (bottom). The inset shows the output power for each case. (d) Optical power and linewidth as functions of current density and number of layers for the case of the III-V/SiN QW laser. (e) Pareto frontier and TOPSIS optimal point of the QW (left) and QD (right) laser diodes.

rate of $10^9$ $s^{-1}$, and a bimolecular recombination rate of $10^{-16}$ $m^3s^{-1}$. The QD and QW devices had cavity lengths of 4 and 0.6 mm, and lateral confinement factors of 0.20 and 0.28, respectively. Fig. 1(b) depicts the eigenmodes of the coupled III-V and SiN cavities showing anticrossing due to optical coupling displaying two resonances, *viz.,* resonance narrow (rn) and resonance wide (rw). Fig. 1(c) shows the effect of varying the number of QD layers (bottom) at a fixed dot density of $4\times10^{14}$ $m^{-2}$ per layer and varying the QD density (top) with 5 QD layers over the lasing linewidth as a function of the injected current density. Moreover, the insets show a colormap of the optical power as a function of both the current density and the QD layers/density. Fig. 2 (c) shows that linewidth narrowing in an integrated III-V/SiN laser occurs in three stages: Immediately pass the lasing threshold, from gain clamping, according to the Schawlow-Townes description; an intermediate region, where locking to the high-Q SiN passive resonator begins to take place; and at sufficiently high injection current, total locking of III-V laser and SiN resonator is achieved, resulting in significant linewidth reduction, up to seven orders of magnitude. Fig. 2(c) also shows that either increasing the QD layers or QD density results in higher optical powers in addition to higher external quantum efficiencies ($\eta_{ext}$) for a given current density. Moreover, increasing the QD layers/density results in the attainment of locking at lower currents. That said, these effects are stronger with increasing the QD density, compared to the number of layers.

Similarly, Fig. 1(d) summarizes the effects of increasing the QW layers on the linewidth as a function of the current density for different layers while the optical power is color coded for each point. Much like the case of the QD device, increasing the QW layers yielded higher optical powers. However, contrary to the case of the QD counterpart, more QW layers resulted in lowering the $\eta_{ext}$ in addition to more stringent locking conditions (higher current injection requirement). The difference in linewidth performance between the QW and QD lasers is attributed to the difference in their linewidth enhancement factors, being near zero in the latter. This is a result of the frequency pulling in QWs being dependent on carrier density, due to their asymmetric carrier density distribution while being independent of carrier density in QDs, due to their symmetric inhomogeneously broadened carrier density distribution.

Lastly, we performed a multi-objective design-performance optimization via a genetic algorithm. The number of QW/QD layers and the current injection are taken as optimization variables. Meanwhile, various objective functions of input power, output power, wall-plug efficiency (WPE), and linewidth FWHM were considered. Then, we followed that with the Technique for Order of Preference by Similarity to Ideal Solution (TOPSIS), a multi-criteria decision-making algorithm [6]. Following this, Fig. 1(e) depicts the 4-dimensional optimization space along the four objective functions for the QW (left) and QD (right) laser, along with the obtained Pareto frontier and the TOPSIS optimal point for each case. For the QW laser, the TOPSIS optimal point was that of an input power of ~54 mW, an output power of ~1.4 mW, an FWHM of ~18 Hz, and a WPE of ~2.6%, manifested with 2 QW layers and a current density of ~2 $kA/cm^2$. The added benefits of increasing either do not outweigh the associated power consumption increase and the efficiency reduction. Therefore, minimizing the number of QW layers and moderate current injection are recommended. Similarly, the TOPSIS optimal point for the QD laser was found to be that of an input power of ~103 mW, an output power of ~0.43 mW, a linewidth of ~67 Hz, and a WPE of ~0.41%, manifested with 8 QD layers and a current density of ~0.5 $kA/cm^2$. In other words, contrary to the III-V/SiN QW laser, maximizing the QD layers yields optimal performance when injected with low currents. The corresponding input power of ~50(100) mW translates into a switching energy consumption of ~5(10) pJ/bit given a 10 Gbit/s data rate in ON-OFF Keying direct modulation.

## 4. Conclusion

A parametric engineering design investigation was presented on the performance of integrated III-V/SiN DFB QW and QD lasers, particularly the linewidth narrowing effect. In addition, a multi-objective optimization based on a genetic algorithm was performed to optimize the design and operation parameters.

## 5. Acknowledgement

This research was supported by Advanced Research Projects Agency-Energy (ARPA-E) No. DE-AR000067, the US Department of Energy under Contract No. DE-AC04-94AL85000 and the American Institute for Manufacturing (AIM) Integrated Photonics.

## 6. References

[1] W. Jin *et al.*, "Hertz-linewidth semiconductor lasers using CMOS-ready ultra-high-Q microresonators," *Nature Photonics,* vol. 15, no. 5, pp. 346-353, 2021.
[2] C. Xiang *et al.*, "Laser soliton microcombs heterogeneously integrated on silicon," *Science,* vol. 373, no. 6550, pp. 99-103, 2021.
[3] C. Xiang *et al.*, "High-performance lasers for fully integrated silicon nitride photonics," *Nature Communications,* vol. 12, no. 1, p. 6650, 2021.
[4] C. Shang *et al.*, "Perspectives on Advances in Quantum Dot Lasers and Integration with Si Photonic Integrated Circuits," *ACS Photonics,* vol. 8, no. 9, pp. 2555-2566, 2021.
[5] W. W. Chow, Y. Wan, J. E. Bowers, and F. Grillot, "Analysis of spontaneous emission limited linewidth of an integrated III-V/SiN laser," *Laser Photonics Rev,* p. 21006620, 2022.
[6] G.-H. Tzeng and J.-J. Huang, *Multiple attribute decision making: methods and applications*. CRC press, 2011.

137.194.127.19 {ts '2023-07-25 19:19:05'}